Structural, optical and magnetic properties of $Zn_{1-x}Mn_xO$ micro-rod arrays synthesized by spray pyrolysis method

S. Yılmaz [a,b], E. Bacaksız [a,*], E. McGlynn [b], İ. Polat [a], Ş. Özcan [c]

[a] Department of Physics, Faculty of Sciences, Karadeniz Technical University, 61080 Trabzon,

Turkey

[b] School of Physical Sciences and National Centre for Plasma Science and Technology, Dublin

City University, Glasnevin, Dublin 9, Ireland

[c] SNTG Lab., Physics Engineering Department, Hacettepe University, Beytepe, 06800 Ankara,

Turkey

* Corresponding author. Tel.: +90 462 377 25 45; fax: +90 462 325 31 95.
E-mail address: eminb@ktu.edu.tr (E. Bacaksız).

Abstract

Undoped and Mn-doped ZnO micro-rod arrays were fabricated by the spray pyrolysis method on glass substrates. X-ray diffraction and scanning electron microscopy showed that these micro-rod arrays had a polycrystalline wurtzite structure and high c-axis preferred orientation. Photoluminescence studies at 10 K show that the increase of manganese content leads to a relative decrease in deep level band intensity with respect to undoped ZnO. Magnetic measurements indicated that undoped ZnO was diamagnetic in nature whereas Mn-doped ZnO samples exhibited ferromagnetic behavior at room temperature, which is possibly related to the substitution of Mn ions (Mn^{2+}) for Zn ions in the ZnO lattice.

1. Introduction

Zinc oxide (ZnO), with a wide direct band gap of 3.37 eV and large exciton binding energy of 60 meV, shows promising materials properties and has attracted intensive research efforts with an emphasis on its possible applications in UV/blue optoelectronics, transparent transistors and photodetectors [1,2]. Doping of ZnO with magnetic ions like Mn, Cr, Fe, Co and Ni results in ferromagnetic semiconductor behavior. In such ferromagnetic semiconductors, a part of the lattice is made up of magnetic atoms and thus they are called diluted magnetic semiconductors (DMS). The term "spintronics" refers to utilizing the spin-degree of freedom of an electron for applications, as opposed to the conventional usage of the charge. Some possible applications of spintronic devices are spin-valve transistors [3], spin light-emitting diodes [4], logic devices [5], and non-volatile memory [6]. The basic requirement for these practical applications is to achieve the Curie temperature (T_C) well above the room temperature [7]. In 2000, Dietl *et al.* predicted theoretically that Mn-doped ZnO and GaN would be ferromagnetic at room temperature and would therefore be suitable for applications in spintronics [8]. Following this initial work, using ab initio calculations based on the local density approximation, Sato *et al.* theoretically demonstrated that V-, Fe-, Co-, Ni- and Cr-doped ZnO showed ferromagnetic ordering above the room temperature [9]. However, a number of experimental studies reveal that the magnetic behavior of Mn in ZnO appear to be dependent on preparation conditions, such as preparation methods, doping concentration, substrate type, substrate temperature and annealing atmosphere. For example, Elanchezhiyan *et al.* observed ferromagnetic behavior for films grown on sapphire substrates while films on Si substrates exhibited only paramagnetic behavior [10]. Work by Pradhan *et al.* indicated that $Zn_{1-x}Mn_xO$ films grown at a substrate temperature of 500 °C exhibited room temperature ferromagnetism and growths beyond 500 °C showed a decrease in the magnetization due to the formation of Mn-related clusters [11]. Furthermore, Cheng *et al.*

reported paramagnetic properties for $Zn_{0.93}Mn_{0.07}O$ films prepared by magnetron sputtering [12], while Fukumura *et al.* observed spin-glass behavior with a strong antiferromagnetic exchange coupling for $Zn_{0.64}Mn_{0.36}O$ films prepared by pulsed laser deposition [13]. Trolio *et al.* demonstrated that the saturation magnetization, M_s, for Mn-doped ZnO increased with Mn concentration up to 4 at.%, while for higher Mn concentrations M_s decreased almost linearly [14]. Finally, Hou *et al.* showed that the net magnetization of Mn-doped ZnO thin films annealed in air decreased, but increased with annealing in inert atmospheres [15]. Although there are many experimental studies on magnetic and non-magnetic doped ZnO films showing room temperature ferromagnetism, the origin of ferromagnetism is still strongly debated in transition metal (TM)-doped oxide DMSs such as ZnO-based DMS [16-18]. Early studies proposed that a free carrier mediated mechanism was responsible for the ferromagnetic behavior [19]. However, more recent studies proposed that native defects like oxygen vacancies give rise to ferromagnetic ordering in oxide based DMS [20].

A considerable research effort has recently been focused on studying TM-doped one-dimensional (1D) ZnO nano/microstructures (such as wires, rods and tubes) due to their potential use in producing nano/microscale spintronic devices [21]. Among the TM ions, the doping of Mn into ZnO is most encouraging since Mn has the highest possible magnetic moment and also the half of the d-band is full, creating a stable fully polarized state [22]. However, determination of the physical origin of magnetic effects in different magnetic ion-doped semiconductors is a crucial factor in development of such materials for wider applications. Different theories of the origin of magnetic effects, including theories based on intrinsic defect involvement as well as the magnetic ion dopants [23], mean that correct control of dopant and defect populations based on such understanding is needed to realize applications. This is one of the aims of the present study.

There are also various methods to fabricate 1D TM-doped ZnO materials. These techniques vapor phase transport [23], hydrothermal method [24], thermal evaporation [25] and spray pyrolysis technique [26]. Among these, the spray pyrolysis is especially suitable, since it has proved to be a simple and inexpensive method, particularly useful for large area applications. Furthermore, there is much less research on the use of spray pyrolysis method for the growth of 1D TM-doped ZnO materials in the literature and the second aim of the present study is to undertake a study of the use and potential of this growth method to grow ZnO-based DMS. In this communication, we present data on ZnO micro-rod arrays synthesized via spray pyrolysis on glass substrates and specifically we have studied the effects of the increase of Mn-doping concentration on ZnO samples using x-ray diffraction (XRD), scanning electron microscopy (SEM), photoluminescence (PL) and magnetic measurements. We have studied the effect of Mn-doping on the visible defect band level in PL, which reduces with increasing Mn-doping, indicating a likely reduction in the number of optically active defects. In addition, magnetic measurements show room temperature ferromagnetism of our Mn-doped ZnO samples. These data allow us to conclude that the ferromagnetism in our samples is not due to defect related ferromagnetism and is likely due to ferromagnetic coupling between Mn^{2+} ions in the lattice, mediated by conduction band electrons. This provides important evidence to help distinguish between different theories (in the case of Mn-doping) for magnetic effects proposed in the literature for magnetic ion-doped ZnO.

2. Experimental details

$Zn_{1-x}Mn_xO$ micro-rod arrays with nominal molar fraction (x) values of 0.00, 0.02, 0.04 and 0.06 were obtained by spray pyrolysis in an air atmosphere. The experimental set up and the other experimental details are described in more detail elsewhere [27]. The initial stock solution

was prepared from zinc chloride ($ZnCl_2$) at 0.1 M concentration in deionized water. Doping was achieved by the addition of $MnCl_2.4H_2O$ (0.1 M) to the stock solution, which was then sprayed on the glass substrate. The growth was performed with a spray rate of about 5 ml/min and the growth rate was ~ 50 nm/min. Prior to growth the glass substrates were cleaned in ethanol and then dried in vacuum. During growth, the substrates were rotated with a speed of 10 rpm and the substrate temperature was kept at 550 °C. XRD data of the samples in θ-2θ mode were taken using a Bruker AXS D8 advance texture diffractometer with CuK_α radiation over the range $2\theta = 20\text{-}60°$ with a step of $0.01°$ at room temperature. The surface morphology and bulk composition were studied with JEOL JSM-6400 SEM equipped with energy dispersive x-ray spectroscopy (EDS) an accelerating voltage of 20 kV and beam current of 50 nA was used in all cases for this study. Optical transmission measurements were performed at room temperature with a Shimadzu UV-1201 UV–VIS–NIR spectrophotometer over a wavelength range of 300–1100 nm. PL measurements were performed at 10 K using a SPEX 1704 monochromator, with a closed cycle cryostat Janis SHI-950-5. PL spectra were excited with the 325 nm line of a He–Cd laser at a power level of ~ 200 mW, unfocussed on the sample surface. Magnetization measurements as a function of magnetic field and temperature were carried out using a Quantum Design Physical Property Measurement System with a vibration sample magnetometer module.

3. Results and discussion

The structural properties of undoped and Mn-doped ZnO micro-rod arrays produced by spray pyrolysis were investigated by XRD, and the results for all samples are shown in Fig. 1(a)-(d). XRD patterns of these samples exhibit peaks corresponding to (100), (002), (101) and (102) planes, which can be indexed as the ZnO powder wurtzite (hexagonal) structure in the standard data (JCPDS, 36-1451). The (002) peak shows the highest intensity in all cases, implying that all

the samples have a hexagonal crystal structure with a preferred orientation with the substrate normal parallel to the normal to the ZnO (002) plane. There were no diffraction peaks detected for Mn metal clusters, Mn oxide secondary phases or other impurity phases within the sensitivity of our XRD measurements, implying that Mn ions were incorporated into the ZnO lattice by substituting on Zn lattice sites. In addition, compared with undoped ZnO sample, increasing the Mn molar fraction caused a shift in diffraction peak position of the Mn-doped ZnO micro-rods. The calculated c values based on the diffraction peak position were found to increase from 5.21 Å for undoped to 5.22 Å for nominally 6 at.% Mn-doped ZnO. The slight increase in the lattice parameter c upon Mn incorporation indicates that samples were in a state of strain and that along the c-axis this strain was tensile [28]. The reason for this c-axis lattice parameter change may be due to the concentration of foreign atoms and the difference of their ionic radii with respect to the substituted matrix ion ions; the radius of Mn^{2+} ions (0.80 Å) is larger than that the Zn^{2+} ions (0.74 Å) or to the differences in the linear thermal expansion coefficients of the ZnO samples with different Mn molar fractions and soda-lime glass [29].

Chemical compositions of undoped and Mn-doped ZnO micro-rods were investigated by EDS. Fig. 2(a) and (b) shows EDS spectra obtained for undoped and nominally 6 at.% Mn doped ZnO micro-rods, respectively, showing the existence of manganese within the samples. Table 1 indicates that all the samples are composed of Zn, O or Mn, demonstrating the increase in concentration with the increase of Mn-doping in ZnO micro-rods. Table 1 also shows that actual atomic percentage ratio of Mn is less than the nominal composition in the solution. The difference between the actual and the nominal Mn concentration is probably due to the dilution of Mn ions in the ZnO host matrix. Additionally, compared to undoped ZnO, it was found that the Mn-doped ZnO micro-rods were slightly zinc deficient and oxygen rich, beyond that expected for

Zn replacement by Mn. Similar results were obtained by Wang *et al.* for Cu-doped ZnO nanoparticle sheets [30].

SEM surface micrographs for the samples are shown in Fig. 3 and reveal that both the undoped and 1.1, 2.6, 4.2 at.% Mn-doped ZnO micro-rod arrays display hexagonal shaped rods with sub-micron diameters. As seen in Fig. 3, the micro-rods in all cases show a distribution of diameters ($3.3 \pm 0.7\,\mu m$, $2.0 \pm 0.5\,\mu m$, $2.2 \pm 0.7\,\mu m$ and $2.5 \pm 1.0\,\mu m$ for the undoped and 1.1, 2.6, 4.2 at.% Mn-doped samples, respectively). However, compared to the undoped ZnO, it was observed that there was no essential change in the morphology of the micro-rods with the increase of Mn-doping. Based on the data from XRD pattern in Fig. 1 and the cross-section image of undoped ZnO sample as illustrated in the inset of Fig. 3(a), the hexagonal rods with a height of ~ 7 μm were found to be regular and almost perpendicular to the substrate, indicating that undoped and Mn-doped ZnO rods preferentially grow along the (002) plane..

The optical transmission spectra at room temperature of the undoped and Mn-doped ZnO micro-rod arrays are shown in Fig. 4(a). The transmittance spectra revealed that all the samples had a low average transmittance below the band gap. The maximum transmission of the undoped ZnO micro-rods was around 25 % and this decreased from 18 % to 10 % with increasing Mn content from x = 0.0 to 4.2 at.%. Krunks *et al.* also reported significantly reduced transmission when ZnO submicron rods were prepared at substrate temperatures exceeding 500 °C by the spray pyrolysis method [31]. On the other hand, Rodriguez-Baez and *et al.* obtained ZnO thin films with a high optical transmittance when the substrate temperature was lower than 500 °C during spray pyrolysis [32]. The smoother surface morphology of those samples and the consequently higher transmittance are fully consistent with our results because of scattering by

the micron-scale roughness of the micro-rod arrays in our sample morphology, as seen in Fig. 2 [33].

Fig. 4(a) also indicates changes in the absorption edge shape and position as the concentration of Mn increases in ZnO micro-rod arrays, which has also been reported in case of Mn-doped ZnO films [34]. One may attempt to determine the optical band gap energy, E_g, from the absorption spectra using a Tauc-plot analysis of the variation of the absorption coefficient (α) with photon energy, utilizing the relation;

$$\alpha(h\nu) = A(h\nu - E_g)^{1/2} \qquad\qquad (1)$$

where E_g is the optical band gap of the films and A is a constant. Fig. 4(b) shows the plots of $(\alpha h\nu)^2$ versus ($h\nu$) for the various ZnO micro-rod array samples. Extrapolations of the linear portions of the plots onto the energy axis were used to estimate the band gap values using this method and these analyses show an apparent decrease in E_g from 3.26 to 2.98 eV with an increase of Mn content from $x = 0.0$ to 4.2 at.%. This behavior in absorption spectra is in agreement to the results reported on Mn-doped ZnO film prepared by other techniques [34-36]. However, we also note that an opposite trend of the band gap energy (as determined by a Tauc plot analysis) increasing with increasing Mn content in ZnO films was also reported in the literature [37,38] and we comment further below on this apparently contradictory results.

In order to investigate the influence of Mn-doping on optical emission and defect formation, PL spectra of undoped and Mn-doped ZnO micro-rods were measured at 10 K and are shown in Fig. 5 (all spectra normalized to the near band edge peak emission). The dominant UV peak seen in all the samples is located at 3.361 eV and is ascribed to the near band edge emission of excitons bound to donors (D^{0}X, members of the so-called I line series) [39]. The energies of

these peaks are identical for all samples, indicating that the dominant donor bound exciton emission energy is unaffected by the Mn incorporation. This D^0X emission is observed at a constant energy below the band gap and thus indicates that the band gaps at low temperatures in all samples are identical, and hence these data are in clear disagreement with the variations in the band gap value determined by the Tauc plots presented above. The low temperature PL data give a very precise value for the band gap due to the sharp emission lines and these data provide clear evidence that the band gaps of all samples are unchanged by Mn incorporation. The origin of this disagreement is easily explained. The Tauc relation in Eq. (1) above assumes free carrier behavior with no electron-hole interactions, whereas for ZnO the large excitonic binding energy of 60 meV means that significant electron-hole correlation is present even at room temperature and the so-called Sommerfeld enhancement factor is clearly seen in absorption spectra at room temperature [40-42]. Thus the use of the Tauc plot analysis is inappropriate for materials such as ZnO, unless correction is made for such excitonic effects. There are clear changes in the absorption edge shape in Fig. 4(a) which indicate a change in the Sommerfeld factor in absorption due to changes in exciton binding/stability and hence excitonic width, rather than a change in band gap. Surprisingly many reports in the literature use the Tauc analysis to determine band gaps in ZnO without taking account of the effects of electron-hole binding and it is likely that this fact, together with changes in the exciton binding/stability due to varying materials quality and defect concentration (as well as Fabry-Perot effects in specular films which are not taken account of) lead to the wide diversity of reported trends in band gap with e.g. Mn doping, as mentioned above [34-38]. For all these reasons we judge the conclusion from the low temperature PL data above, i.e. that the band gaps of the samples are unaffected by Mn doping, to be the correct one.

The undoped ZnO sample exhibits three sharp peaks located at 3.287 eV, 3.219 eV and 3.146 eV, respectively. These peaks may be due to more tightly bound excitons but we note also that the spacing between them corresponds closely to the longitudinal-optical phonon energy of ~ 72 meV, so that at least some of them may be due to phonon replicas [43]. After doping the ZnO micro-rods with Mn, these peaks are not longer seen [44]. In the deep level region, as shown in the inset of Fig. 5, all the samples display a defect-related visible luminescence band, which is usually related to defects such as zinc interstitials (Zn_i) and oxygen vacancies (V_o) [29]. The relative intensity of this band (compared to the band edge peak at 3.361 eV) decreased with increased Mn-doping level, which may be due to the decreasing number of the optically active defects as well as the thermal quenching as a result of the increase in the nonradiative transition centers created by Mn incorporation and intrinsic defects mentioned previously [45-47]. Kuhnert *et al.* obtained a similar quenching effect after doping with different donor impurities and explained that donor doping shifted the Fermi level above the Cu^{2+} level so that the hole was no longer stable in the *d* shell, giving rise to the quenching of the green luminescence band [48].

Magnetization versus magnetic field (M-H) curves of the micro-rod arrays corresponding to the actual Mn-dopant molar fractions x = 0.0, 1.1, 2.6 and 4.2 at.% measured at 300 K are shown in Fig. 6. The diamagnetic contribution from the substrate is subtracted from the total magnetization. As illustrated in the upper left inset of Fig. 6, undoped ZnO sample exhibited diamagnetic behavior. A similar result was obtained by Liu *et al.* for pure ZnO in In-doped ZnO nanowires grown by vapor phase transport process [49]. It is clear that all Mn-doped ZnO samples showed ferromagnetic behavior at room temperature but the 2.6 at.% Mn-doped ZnO showed stronger ferromagnetic behavior than either the 1.1 at.% Mn- or 4.2 at.% Mn-doped samples. The coercive field (H_c) and the remnant magnetization (M_r) of 2.6 at.% Mn-doped ZnO micro-rods are found to be ~ 15 kA/m and ~ 100 A/m, respectively. However, these (H_c and M_r)

11

values decreased to ~ 11 kA/m, ~ 80 A/m for 1.1 at.% Mn and ~ 10.5 kA/m, ~ 60 A/m for 4.2 at.% Mn-doped ZnO samples. Additionally, 1.1 at.%, 2.6 at.% and 4.2 at.% Mn-doped ZnO micro-rods almost exhibited stable M_s values of ~ 39, ~ 57 and ~ 59 A/m, respectively.

In order to explain the origin of room temperature ferromagnetism, several experimental research groups made some studies on Mn-doped ZnO. For example, Elanchezhiyan et $al.$ observed a maximum ferromagnetic moment for their 5 at.% Mn-doped ZnO thin films and found that the ferromagnetic nature decreases with an increase in Mn concentration. They attributed this to the clustering of Mn ions, which causes a decrease in Mn–Mn distance leading to decrease in ferromagnetic behavior [50]. However, Yan et $al.$ pointed out that oxygen vacancies play an important role in the appearance of room temperature ferromagnetism for Mn-doped ZnO nanorods [51]. Ramachandran et $al.$ also suggested that the origin of room temperature ferromagnetism observed for Mn:ZnO samples was related to carrier or defect mediated mechanism [52]. Furthermore, Cong et $al.$ proposed that magnetic behaviour of Mn-doped ZnO nanostructures can be explained by carrier induced mechanism, implying the exchange interaction between local spin-polarized electrons (such as the electrons of Mn^{2+} ions) and conductive electrons [53]. Dietl et $al.$ also described the origin of the ferromagnetism in Co-doped ZnO in terms of a spinodal decomposition of a Co-rich antiferromagnetic nanocrystals embedded in a paramagnetic matrix of ZnO:Co. They concluded that the observed room temperature ferromagnetism resulted from uncompensated spins at the antiferromagnetic nanocrystal surfaces [54].

Mn, MnO_2 and Mn_2O_3 are antiferromagnetic with a Neel temperatures (T_N) of ~ 100 K, ~ 84 K and ~ 75 K, respectively while Mn_3O_4 is ferromagnetic with a T_C of ~ 43 K [55]. In regard to the origin of the ferromagnetism observed in our samples, since these Mn-related phases weren't observed in our samples by XRD measurements, it appears that the origin of the room

temperature ferromagnetism in the samples are not due to presence of manganese oxides or clusters. According to the PL results already discussed, the relative intensity of the deep level band for Mn-doped ZnO samples is smaller than that of undoped ZnO, indicating that Mn-doping may decrease the concentration of defects such as V_o and Zn_i. Hence, we can pronounce that the origin of the observed ferromagnetism of our samples cannot be attributed to defect-related ferromagnetism. Additionally, since there is a correlation between the observed ferromagnetism and carriers (discussed later), neither antiferromagnetism (with a T_N of 300 K) nor superparamagnetism were seen in our Mn-doped ZnO samples that therefore we conclude that the origin of the ferromagnetism cannot ascribe to the spinodal decomposition [56,57]. Therefore we consider that the observed room temperature ferromagnetism of our samples most probably result from the substitution of Mn ions (Mn^{2+}) for Zn ions in the ZnO lattice, which was indicated by XRD results. It was reported that Mn^{2+} had an important effect in the ferromagnetic properties of Mn-doped ZnO [58]. According to Ruderman-Kittel-Kasuya-Yosida theory [59,60], the magnetism originate from the exchange interaction between local spin-polarized electrons (such as the electrons of Mn^{2+} ions) and conduction electrons. This interaction leads to the spin polarization of conductive electrons and subsequently, the spin-polarized conductive electrons perform an exchange interaction with local spin-polarized electrons of other Mn^{2+} ions. Thus after the long-range exchange interaction, almost all Mn^{2+} ions exhibit the same spin direction. The conduction electrons are regarded as a medium to "connect" all Mn^{2+} ions. As a result, the material exhibits ferromagnetism [22].

It was also found that M_r value initially increased with 2.6 at.% Mn-doping content and then decreased for 4.2 at.% Mn-doped ZnO sample, indicating a deterioration in the ferromagnetism for 4.2 at.% Mn-doped ZnO. This can be explained by the ferromagnetic-antiferromagnetic competition, saying that at higher concentrations may be ascribed to an

increasing occurrence of antiferromagnetic coupling for Mn pairs happening at shorter separation distances, leading to a decreasing the ferromagnetic interaction, which was reported in the literature previously also [38,50,61].

The magnetization versus temperature (M–T) curve was measured at a temperature range of 5–300 K and is shown in Fig. 7. These data show that the temperature dependence of the magnetization of the 2.6 at.% Mn-doped ZnO sample is linear at high temperatures. At lower temperatures it displays a steep rise with pronounced concave curvature but without showing any distinct magnetic phase transition. A strong deviation from the linear behavior at low temperature can be attributed to antiferromagnetic behavior originating from the Mn-Mn exchange interaction [62]. Based on these data we can conclude that the T_C is well above room temperature, but it is hard to determine the exact value, since it exceeds the temperature range of our measurements. Quite a number of previous works have shown that Mn-doped ZnO displays ferromagnetism with T_C values of about 30-40 K [63,64], while others have observed T_C values above room temperature, the latter in agreement with our results [65].

4. Conclusions

Based on the structural, optical and magnetic measurements shown and discussed above, the following conclusions can be drawn: (i) all the samples have a hexagonal structure with a strong [002] preferred orientation normal to the substrate, Mn incorporation did not significantly change the texture or the morphology but did lead to a slight increase in c-axis lattice constant (ii) compared to the undoped ZnO, the number of optically active deep level defects decreased for Mn-doped ZnO micro-rod samples; (iii) the different Mn-doped ZnO micro-rod arrays displayed ferromagnetic loops clearly, though a quantitative estimation of the T_C was not possible. Based on these data we can conclude that the ferromagnetism in our samples is not due to defect-related

ferromagnetism and is likely due to ferromagnetic coupling between Mn^{2+} ions in the lattice which provides evidence to help distinguish between different theories for magnetic effects proposed in the literature in the case of Mn-doped ZnO.

Figure Captions

Fig. 1. XRD patterns of (a) undoped, (b) 1.1 at.% Mn-, (c) 2.6 at.% Mn- and (d) 4.2 at.% Mn-doped ZnO micro-rod arrays.

Fig. 2. EDS spectra of (a) undoped and (b) 4.2 at.% Mn doped ZnO micro-rod arrays.

Fig. 3. SEM images of (a) undoped and the inset shows a cross-section image of the undoped ZnO, (b) 1.1 at.% Mn-, (c) 2.6 at.% Mn- and (d) 4.2 at.% Mn-doped ZnO micro-rod arrays.

Fig. 4. (a) Optical transmission spectra of undoped, 1.1 at.% Mn-, 2.6 at.% Mn- and 4.2 at.% Mn-doped ZnO micro-rod arrays, (b) Plots of $(\alpha h\upsilon)^2$ versus $(h\upsilon)$ for undoped, 1.1 at.% Mn-, 2.6 at.% Mn- and 4.2 at.% Mn-doped ZnO micro-rod arrays.

Fig. 5. PL spectra of undoped, 1.1 at.% Mn-, 2.6 at.% Mn and 4.2 at.% Mn-doped ZnO micro-rod arrays as recorded at 10 K. Inset shows deep level band in magnified view.

Fig. 6. Room temperature (M-H) curves of undoped, 1.1 % Mn-, 2.6 % Mn- and 4.2 % Mn-doped ZnO micro-rod arrays. Upper left inset shows (M-H) curve of undoped ZnO sample.

Fig. 7. (M-T) curve of 2.6 at.% Mn-doped ZnO micro-rod arrays.

Table captions

Table 1. Actual atomic concentrations of Zn, O or Mn in undoped and nominally 2 at.% Mn-, 4 at.% Mn- and 6 at.% Mn-doped ZnO micro-rod arrays.

References

[1] A. Janotti, C.G. Van de Walle, Rep. Prog. Phys. 72 (2009) 126501.

[2] E. Lee, D. Moon, J.H. Yang, K.S. Lim, Y.K. Choi, IEEE Electron Device Lett. 30 (2009) 493.

[3] J.K. Furdyna, J. Appl. Phys. 64 (1988) R29.

[4] S.J. Pearton, W.H. Heo, M. Ivill, D.P. Norton, T. Steiner, Semicond. Sci. Technol. 19 (2004) R59.

[5] Y.X. Wang, H. Liu, Z.Q. Li, X.X. Zhang, R.K. Zheng, S.P. Ringer, Appl. Phys. Lett. 89 (2006) 042511.

[6] S.W. Jung, S.J. An, G.C. Yi, Appl. Phys. Lett. 80 (2002) 4561.

[7] D.A. Schwartz, D.R. Gamelin, Adv. Mater. 16 (2004) 2115.

[8] T. Dietl, H. Ohno, F. Matsukura, J. Cibert, D. Ferrand, Science 287 (2000) 1019.

[9] K. Sato, H. Katayama-Yoshida, Semicond. Sci. Technol. 17 (2002) 367.

[10] J. Elanchezhiyan, K.P. Bhuvana, N. Gopalakrishnan, T. Balasubramanian, J. Alloys Compd. 463 (2008) 84.

[11] A.K. Pradhan, K. Zhang, S. Mohanty, J.B. Dadson, D. Hunter, Appl. Phys. Lett. 86 (2005) 152511.

[12] X.M. Cheng, C.L. Chien, J. Appl. Phys. 93 (2003) 7876.

[13] T. Fukumura, Z. Jin, M. Kawasaki, T. Shono, T. Hasegawa, H. Koinuma, Appl. Phys. Lett. 78 (2001) 958.

[14] A.D. Trolio, C. Veroli, A.M. Testa, D. Fiorani, Superlattices Microstruct. 46 (2009) 101.

[15] D.L. Hou, X.J. Ye, H.J. Meng, H.J. Zhou, X.L. Li, C.M. Zhen, G.D. Tang, Mater. Sci. Eng. B 138 (2007) 184.

[16] M. Chakrabarti, S. Dechoudhury, D. Sanyal, T.K. Roy, D. Bhowmick, A. Chakrabarti, J. Phys. D: Appl. Phys. 41 (2008) 135006.

[17] Z.X. Cheng, X.L. Wang, S.X. Dou, K. Ozawa, H. Kimura, P. Munroe, J. Phys. D: Appl. Phys. 40 (2007) 6518.

[18] B.B. Straumal, S.G. Protasova, A.A. Mazilkin, A.A. Myatiev, P.B. Straumal, G. Schütz, E. Goering, B. Baretzky, J. Appl. Phys. 108 (2010) 073923.

[19] K. Sato, H. Katayama-Yoshida, Jpn. J. Appl. Phys. Part 2 39 (2000) L555.

[20] J.M.D. Coey, A.P. Douvalis, C.B. Fitzgerald, M. Venkatesan, Appl. Phys. Lett. 84 (2004) 1332.

[21] H. Ohno, Science 281 (1998) 951.

[22] P. Sharma, A. Gupta, K.V. Rao, F.J. Owens, R. Sharma, R. Ahuja, J.M.O. Guillen, B. Johansson, G.A. Gehring, Nat. Mater. 2 (2003) 673.

[23] S. Yılmaz, E. McGlynn, E. Bacaksız, Ş. Özcan, D. Byrne, M.O. Henry, R.K. Chellappan, J. Appl. Phys. 111 (2012) 013903.

[24] Y. Zuo, S. Ge, Z. Chen, L. Zhang, X. Zhou, S. Yan, J. Alloys Compd. 470 (2009) 47.

[25] K.-H. Zheng, Z. Liu, J. Liu, L.-J Hu, D.-W. Wang, C.-Y. Chen, L.-F. Sun, Chin. Phys. B 19 (2010) 026101.

[26] E. Bacaksiz, M. Altunbaş, S. Özçelik, O. Oltulu, M. Tomakin, S. Yılmaz, Mater. Sci. Semicond. Process. 12 (2009) 118.

[27] E. Bacaksiz, S. Aksu, S. Yılmaz, M. Parlak, M. Altunbaş, Thin Solid Films 518 (2010) 4076.

[28] H. Deng, J.J. Russell, R.N. Lamb, B. Jiang, Thin Solid Films 458 (2004) 43.

[29] H. Morkoç, Ü. Özgür, Zinc Oxide: Fundamentals, Materials and Device Technology, Wiley-Vch Verlag GmbH & Co. KGaA, Weinheim, 2009, p.4.

[30] R.C. Wang, H.Y. Lin, Mater. Chem. Phys. 125 (2011) 263.

 [31] M. Krunks, T. Dedova, I.O. Açik, Thin Solid Films 515 (2006) 1157.

[32] J. Rodriguez-Baez, A. Maldonado, G. Torres-Delgado, R. Castanedo-Perez, M. De la, L. Olvera, Mater. Lett. 60 (2006) 1594.

[33] J.H. Lee, B.W. Yeo, B.O. Park, Thin Solid Films 457 (2004) 333.

[34] V.R. Shinde, T.P. Gujar, C.D. Lokhande, R.S. Mane, S.H. Han, Mater. Chem. Phys. 96 (2006) 326.

[35] S. Senthilkumaar, K. Rajendran, S. Banerjee, T.K. Chini, V. Sengodan, Mater. Sci. Semicond. Process. 11 (2008) 6.

[36] Y. Caglar, S. Ilican, M. Caglar, F. Yakuphanoglu, J. Sol-Gel Sci. Technol. 53 (2010) 372.

[37] H.K. Yadav, K. Sreenivas, V. Gupta, J. Appl. Phys. 99 (2006) 083507.

[38] H.Y. Xu, Y.C. Liu, C.S. Xu, Y.X. Liu, C.L. Shao, R. Mu, J. Chem. Phys. 124 (2006) 074707.

[39] B.K. Meyer, H. Alves, D.M. Hofmann, W. Kriegseis, D. Forster, F. Bertram, J. Christen, A. Hoffmann, M. Straßburg, M. Dworzak, U. Haboeck, A.V. Rodina, Phys. Status Solidi b 241 (2004) 231.

[40] R.J. Elliott, Phys. Rev. 108 (1957) 1384.

[41] W.Y. Liang, A.D. Yoffe, Phys. Rev. Lett. 20 (1968) 59.

[42] C.F. Klingshirn, Semiconductor Optics, (3rd Edition), Springer, Berlin, 2006.

[43] D.C. Reynolds, D.C. Look, B. Jogai, R.L. Jones, C.W. Litton, W. Harsch, G. Cantwell, J. Lumin. 82 (1999) 173.

[44] X.T. Zhang, Y.C. Liu, J.Y. Zhang, Y.M. Lu, D.Z. Shen, X.W. Fan, X.G. Kong, J. Cryst. Growth 254 (2003) 80.

[45] Ü. Özgür, Y.I. Alivov, C. Liu, A. Teke, M.A. Reshchikov, S. Dogan, V. Avrutin, S.J. Cho, H. Morkoc, J. Appl. Phys. 98 (2005) 041301.

[46] D.C. Look, G.C. Farlow, P. Reunchan, S. Limpijumnong, S.B. Zhang, K. Nordlund, Phys. Rev. Lett. 95 (2005) 225502.

[47] D. Shuang, X.X. Zhu, J.B. Wang, X.L. Zhong, G.J. Huang, C. He, Appl. Surf. Sci. 257 (2011) 6085.

[48] R. Kuhnert, R. Helbig, J. Lumin. 26 (1981) 203.

[49] K.W. Liu, M. Sakurai, M. Aono, J. Appl. Phys. 108 (2010) 043516.

[50] J. Elanchezhiyan, K.P. Bhuvana, N. Gopalakrishnan, T. Balasubramanian, Mater. Lett. 62 (2008) 3379.

[51] H.L. Yan, X.L. Zhong, J.B. Wang, G.J. Huang, S.L. Ding, G.C. Zhou, Y.C. Zhou, Appl. Phys. Lett. 90 (2007) 082503.

[52] S. Ramachandran, J. Narayan, J.T. Prater, Appl. Phys. Lett. 88 (2006) 242503.

[53] C.J. Cong, K.L. Zhang, Phys. Status Solidi b 243 (2006) 2764.

[54] T. Dietl, T Andrearczyk, A. Lipiska, M. Kiecana, M. Tay, Y. Wu, Phys Rev B 76 (2007) 155312.

[55] J.M. Baik, J.L. Lee, Adv. Mater. 17 (2005) 2745.

[56] L.R Shah, H. Zhu,W.G. Wang, B. Ali, T. Zhu, X. Fan, Y.Q. Song, Q.Y. Wen, H.W. Zhang, S.I. Shah, J.Q. Xiao, J. Phys. D: Appl. Phys. 43 (2010) 035002.

[57] M.A. White, S.T. Ochsenbein, D.R. Gamelin, Chem. Mater. 20 (2008) 7107.

[58] Y.B. Lin, J.P. Xu, W.Q. Zou, L.Y. Lv, Z.H. Lu, F.M. Zhang, Y.W. Du, Z.G. Huang, J.G. Zheng, J. Phys. D: Appl. Phys. 40 (2007) 3674.

[59] M.A. Ruderman, C. Kittel, Phys. Rev. 96 (1954) 99.

[60] K. Yosida, Phys. Rev. 106 (1957) 893.

[61] W. Chen, L.F. Zhao, Y.Q. Wang, J.H. Miao, S. Liu, Z.C. Xia, S.L. Yuan, Appl. Phys. Lett. 87 (2005) 042507.

[62] Dhananjay, J. Nagarajua, S.B. Krupanidhi, Mater. Sci. Eng. B 133 (2006) 70.

[63] J.J. Liu, M.H. Yu, W.L. Zhou, J. Appl. Phys. 99 (2006) 08M119.

[64] Y.Q. Wang, S.L. Yuan, Y.X. Song, L. Liu, Z.M. Tian, P. Li, Y.M. Zhou, Y.L. Li, S.Y. Yin, Chinese Sci. Bull. 52 (2007) 1019.

[65] U. Philipose, S.V. Nair, S. Trudel, C.F. De Souza, S. Aouba, R.H. Hill, H.E. Ruda, Appl. Phys. Lett. 88 (2006) 263101.

Tables (if any)

Table 1

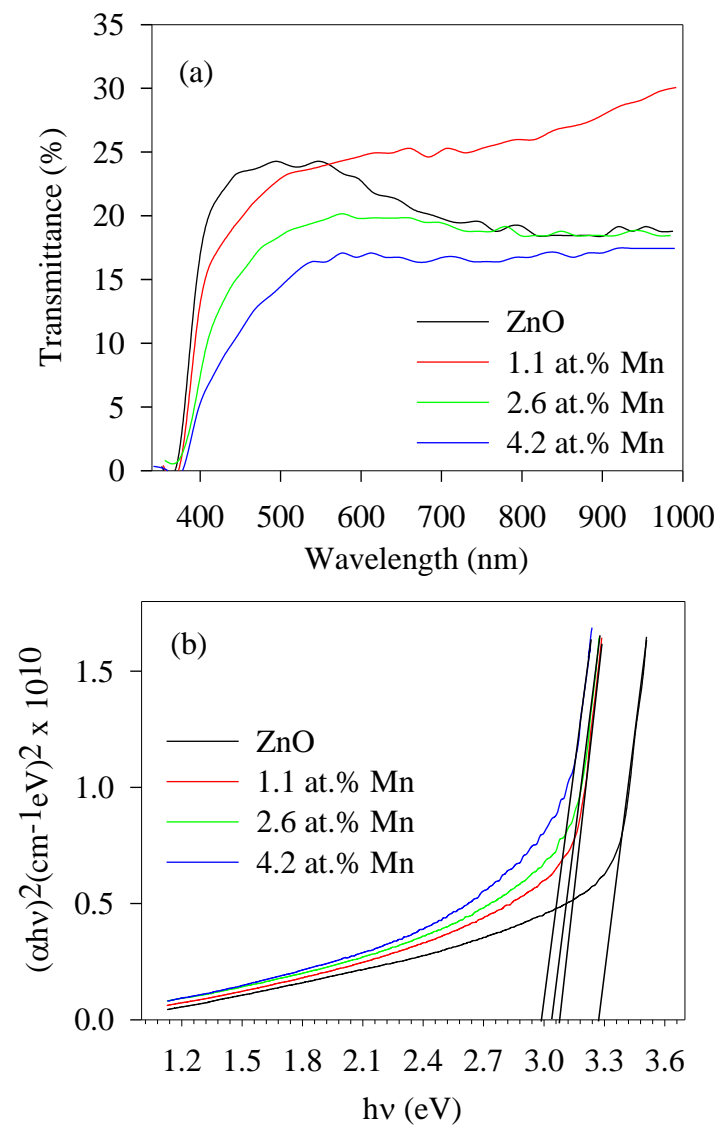| Sample	Measured at.%		
	Mn	Zn	O
ZnO	-	49.0	51.0
2 at.% (nominal) Mn-doped ZnO	1.1	45.3	53.6
4 at.% (nominal) Mn-doped ZnO	2.6	42.9	54.5
6 at.% (nominal) Mn-doped ZnO	4.2	42.1	53.7
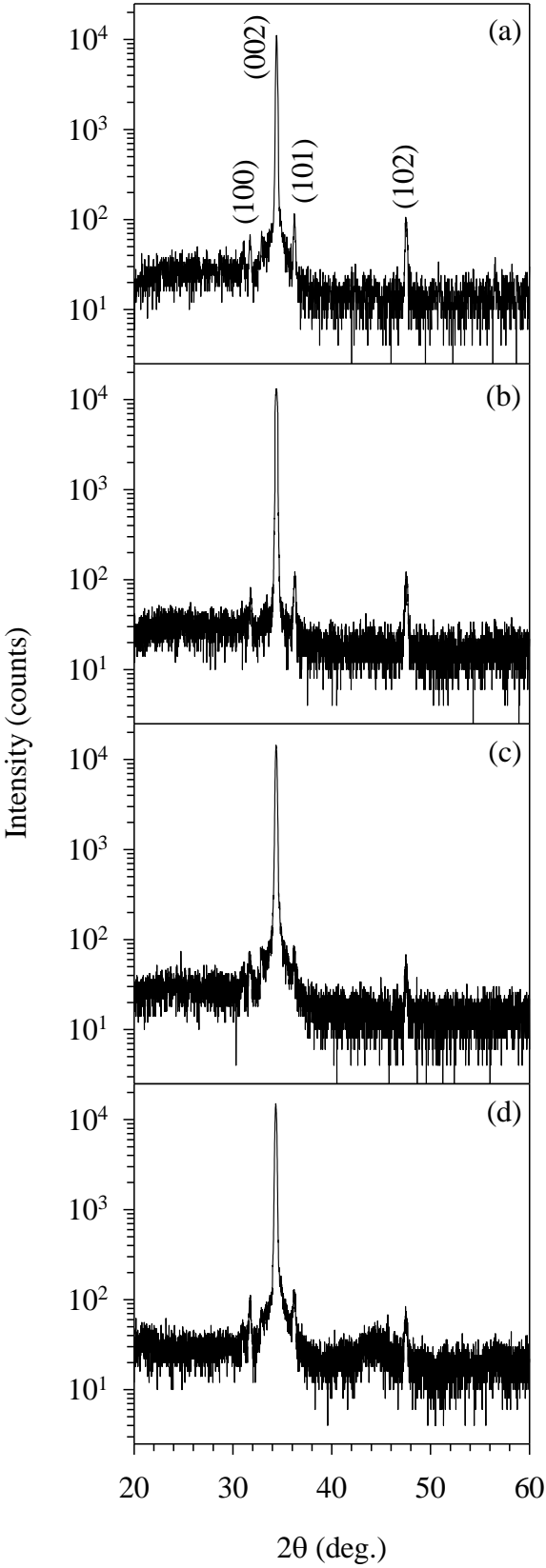
Fig. 1
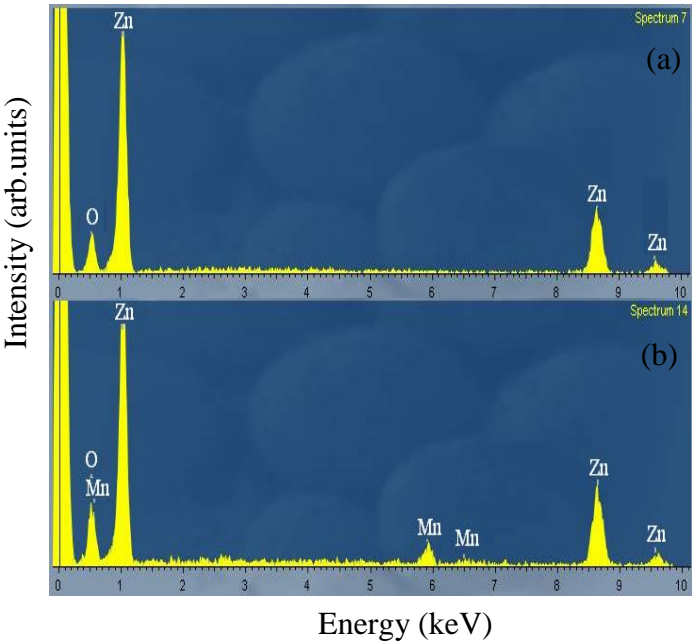
Fig. 2

Fig. 3

Fig. 4

Fig. 5

Fig. 6

Fig. 7